Determination of the chiral condensate from QCD Dirac spectrum on the lattice

H. Fukaya,[1] S. Aoki,[2,3] T. W. Chiu,[4] S. Hashimoto,[5,6] T. Kaneko,[5,6] J. Noaki,[5] T. Onogi,[1] and N. Yamada[5,6]

(JLQCD and TWQCD collaborations)

[1]*Department of Physics, Osaka University, Toyonaka 560-0043, Japan*
[2]*Graduate School of Pure and Applied Sciences, University of Tsukuba, Tsukuba, Ibaraki 305-8571, Japan*
[3]*Center for Computational Sciences, University of Tsukuba, Tsukuba, Ibaraki 305-8577, Japan*
[4]*Physics Department and Center for Quantum Science and Engineering, National Taiwan University, Taipei 10617, Taiwan*
[5]*KEK Theory Center, High Energy Accelerator Research Organization (KEK), Tsukuba 305-0801, Japan*
[6]*School of High Energy Accelerator Science, The Graduate University for Advanced Studies (Sokendai), Tsukuba 305-0801, Japan*

We calculate the chiral condensate of QCD with 2, 2 + 1, and 3 flavors of sea quarks. Lattice QCD simulations are performed employing dynamical overlap fermions with up- and down-quark masses covering a range between 3 and 100 MeV. On $L \sim 1.8$–1.9 fm lattices at a lattice spacing ~ 0.11 fm, we calculate the eigenvalue spectrum of the overlap-Dirac operator. By matching the lattice data with the analytical prediction from chiral perturbation theory at the next-to-leading order, the chiral condensate in the massless limit of up and down quarks is determined.

I. INTRODUCTION

Chiral condensate Σ in quantum chromodynamics (QCD) is not a directly accessible quantity in experiment, yet it plays a crucial role in the low-energy dynamics of QCD as an order parameter of chiral symmetry breaking. When Σ in the limit of massless quarks is nonzero, chiral symmetry is spontaneously broken and hadrons acquire a mass of order Λ_{QCD}, the QCD scale. Only the pion remains massless as the Nambu-Goldstone boson; its dynamics are well described by an effective theory known as chiral perturbation theory (ChPT) [1,2]. Σ is one of the two most fundamental parameters in ChPT (the other is the pion decay constant F) and appears in the predictions of various physical quantities.

Calculation of Σ, the expectation value of the scalar density operator $\Sigma = -\langle \bar{q}q \rangle$, from the first principles of QCD requires nonperturbative techniques. In this paper we report on a numerical calculation of Σ in lattice QCD including the effects of up, down, and strange sea quarks. We investigate the low-lying eigenvalue spectrum $\rho(\lambda)$ of the Dirac operator, which is related to Σ through the Banks-Casher relation $\rho(0) \rightarrow \Sigma/\pi$ [3] and its extension to the case of nonzero λ. Since only the low-lying eigenvalues are relevant, one can avoid contamination from ultraviolet divergence of the scalar density operator $\bar{q}q$, which is of order m/a^2 at a finite quark mass m and a lattice spacing a.

The Banks-Casher relation is satisfied in the limit of massless quarks after taking the large volume limit (the thermodynamical limit), which is the meaning of the arrow in the relation $\rho(0) \rightarrow \Sigma/\pi$. When the massless limit is taken at a finite volume, the vacuum expectation value of $\bar{q}q$ shows a critical fluctuation which leads to a divergent correlation length and vanishing chiral condensate. Taking the thermodynamical limit, on the other hand, is numerically expensive in practical lattice calculations. In this study, we use the low-energy effective theory as a guidance of volume and quark mass scalings. Namely, once the scaling behavior predicted by the effective theory is confirmed by the lattice data, the infinite volume and chiral limit according to the scaling can be safely taken. The scaling we consider is that for varying the eigenvalue λ, volume V, and the quark mass m.

We use the ChPT formula for the low-lying eigenvalue spectrum of the Dirac operator [4], which is valid in both the p and ϵ regimes. The ϵ regime is a parameter region where the quark mass is so small that the Compton wavelength of the pion is longer than the extent of the finite-volume space-time. In this regime, the constant mode of the pion field has to be integrated out over the group manifold when the path integral is evaluated, which is a nonperturbative calculation in the sense that one does not use the expansion in small pion field. At the leading order of the so-called ϵ expansion, the system is equivalently described by the chiral random matrix theory (ChRMT), with which a number of theoretical predictions for the low-lying Dirac spectrum have been derived [5–8]. In the other regime (p regime), where the pion Compton wavelength fits in the volume, the conventional ChPT applies and the calculation of the Dirac operator spectrum is available as well [9,10]. The new method given in [4] consistently combines the both results within a systematic expansion, and thus is valid in both regimes as well as in between. By lattice calculations, we produce the data at various sets of quark masses to firmly test this analytic expectation.

Application of the ChPT formula for the low-lying Dirac spectrum requires a good control of the chiral symmetry in the calculation. In this work, we use the overlap-Dirac operator [11,12] which satisfies the Ginsparg-Wilson relation [13] and thus realizes a *modified* chiral symmetry on the lattice [14]. Since the chiral effective theory is constructed only assuming the presence of chiral symmetry, the same construction as in the continuum theory can be applied to lattice QCD with overlap fermions. Although the overlap-Dirac eigenvalues lie on a circle on the complex plane, the physical imaginary part is uniquely identified up to $O(a^2)$ discretization effects.

In our previous works [15,16] we performed large-scale lattice simulations of two-flavor QCD using the overlap fermion formulation [17] and calculated low-lying Dirac eigenvalues. By matching the lowest eigenvalue spectrum with the ChRMT expectations, we extracted Σ. Since the ChRMT corresponds to the leading order of the ϵ expansion in ChPT, this result is subject to NLO or $O(1/F^2 V^{1/2})$ corrections, which could be sizable on the lattice of size $V = L^3 T \sim (1.9 \text{ fm})^4$ used in that study. Another limitation was that the quark mass must be very small to apply the ϵ regime formula, and the runs in the p regime could not be used in the analysis.

Application of the new formula [4] is attempted for the first time in our recent work [18,19] in which next-to-leading-order (NLO) corrections are included in the analysis. Using the $2 + 1$-flavor QCD data generated with dynamical overlap fermions on $16^3 \times 48$ lattices, the value of Σ in the chiral limit of two light quarks is obtained. The present paper provides an extensive description of this work.

In this paper, we analyze the low-lying Dirac spectrum mainly on the $2 + 1$-flavor QCD simulations, where the strange quark mass m_s is fixed near its physical value. The mass of degenerate up and down quarks, m_{ud}, covers a range between $m_s/5$ and m_s in the p regime lattice ensembles, which are generated for calculations of various physical quantities including the pion mass and decay constant [20]. We also generate an ϵ regime ensemble, where the up and down quarks are kept nearly massless while m_s is fixed near the physical value. The NLO ChPT formula allows us to combine these data to obtain Σ in the chiral limit of up and down quarks. We also extract the pion decay constant F and one of the NLO low energy constants (LECs) L_6 from the correction terms.

As demonstrated in the following sections, the ChPT formula provides information on the shape of the low-lying Dirac spectrum, with which we can test the agreement between the formula and the lattice data in detail. The volume dependence gives a critical test, since it is essentially controlled by Σ and F. At some parameter points, we compare the data obtained on a larger ($24^3 \times 48$) lattice to those on the smaller ($16^3 \times 48$) volume to check if the ChPT prediction consistently describes the difference.

The sea quark mass dependence of the chiral condensate is partly controlled by L_6 but we also expect a nonanalytic dependence due to the pion-loop effects that should be observed in the lattice data. These nontrivial consistency checks are performed to gain confidence in the final result for Σ.

In addition to the main analysis in $2 + 1$-flavor QCD, we also investigate two-flavor QCD and three-flavor QCD where m_{ud} and m_s are degenerate. For the case of two-flavor QCD, the lattice data are the same as in our previous studies [15,16], but we use the ChPT formula valid at NLO in this new analysis. The degenerate three-flavor QCD configurations are newly generated for this study at two light quark masses. We thus obtain the chiral condensate Σ for these variants of QCD.

This paper is organized as follows. In Sec. II, we briefly explain how the chiral condensate is determined from the Dirac eigenvalue density and how the finite volume effects are removed using ChPT. Some technical aspects of lattice QCD simulations are described in Sec. III and the numerical results are discussed in the following sections. First, we describe the strategy to extract the LECs from lattice data of the spectral density in Sec. IV. Second, numerical scaling tests of the NLO ChPT formula are presented in Sec. V. We then proceed to the determination of Σ in the chiral limit in Sec. VI. Summary of this analysis and conclusions are given in Sec. VII.

II. BANKS-CASHER RELATION IN A FINITE-VOLUME

Eigenvalues of the Dirac operator in four-dimensional continuum Euclidean space are pure imaginary (which we denote $i\lambda_1, i\lambda_2, \cdots$ with real λ_i's). The spectral density at an eigenvalue $i\lambda$ is defined by

$$\rho(\lambda) \equiv \frac{1}{V} \sum_{k}^{\infty} \langle \delta(\lambda - \lambda_k) \rangle, \tag{1}$$

where $\langle \cdots \rangle$ denotes an average over the gauge configuration space. Since a nonzero eigenvalue appears as a pair with its complex conjugate, $\rho(\lambda) = \rho(-\lambda)$, we only consider the $\lambda \geq 0$ region in the following.

The chiral condensate Σ in the limit of massless quarks and infinite volume is an order parameter of the chiral symmetry breaking. Through the Banks-Casher relation [3], Σ is related to $\rho(\lambda)$ as

$$\lim_{m \to 0} \lim_{V \to \infty} \rho(0) = \frac{\Sigma}{\pi}, \tag{2}$$

with which one can identify the spontaneous breaking of chiral symmetry by measuring $\rho(0)$ instead of Σ.

Even when the volume V, sea quark masses $\{m_{\text{sea}}\} = \{m_u, m_d, m_s, \cdots\}$ and λ are all finite, a similar nonperturbative relation,

$$\rho(\lambda) = -\mathrm{Re}\frac{\langle\bar{q}q\rangle}{\pi}\bigg|_{m_v=i\lambda}, \qquad (3)$$

holds. Here, $(\cdots)|_{m_v=i\lambda}$ means that the quantity is evaluated with the valence quark mass analytically continued to a pure imaginary value $i\lambda$. In this relation, the ultraviolet divergence in the definition of the $\bar{q}q$ operator cancels by taking its real part at an imaginary value $m_v = i\lambda$ (where the divergent part is pure imaginary), which is natural because the left-hand side of the equation only refers to low-lying modes and is insensitive to the ultraviolet region of the dynamics.

We note that the relation (3) is valid even when the ensemble average $\langle\cdots\rangle$ is restricted to a given topological sector of Q in the gauge field configurations [21], that we denote $\langle\cdots\rangle_Q$. Namely, if we define the spectral density at a given topological sector as $\rho_Q(\lambda) \equiv (1/V)\sum_k\langle\delta(\lambda - \lambda_k)\rangle_Q$, it is obtained by computing $-\mathrm{Re}\langle\bar{q}q\rangle_Q/\pi$.

Although the chiral condensate Σ is different from $-\mathrm{Re}\langle\bar{q}q\rangle|_{m_v=i\lambda}$ at finite volumes, the difference can be described by the low-energy effective theory, provided that the energy scales of the theory are well below the QCD scale:

$$\lambda, \quad m_i, \quad 1/V^{1/4} \ll \Lambda_{\mathrm{QCD}}. \qquad (4)$$

It is, therefore, possible to directly compare the lattice QCD calculation of $\rho(\lambda)$ at finite λ, m_i, Q, and V with the prediction of the effective theory. By taking the limit of $m_i \to 0$ after $V \to \infty$ according to the effective theory and summing over Q, one can reproduce the physical $\rho(\lambda)$, which in the limit of $\lambda \to 0$ gives Σ.

In this direction, studies in both lattice QCD [22–28] and the low-energy effective theory have been done. Smilga and Stern [9] and Osborn *et al.* [10] calculated the Dirac eigenvalue spectrum in the conventional p expansion of (partially quenched) ChPT to NLO. In the vicinity of $\lambda = 0$, which corresponds to the limit of zero valence pion mass, a special treatment of the zero-momentum modes is needed because the correlation length exceeds the size of the volume. This special treatment is known as the ϵ expansion of ChPT, in which the zero-momentum modes are nonperturbatively integrated over the $SU(N_f)$ (or $U(N_f)$ when the topological charge Q is fixed) manifold. At the leading order (LO), the finite size effect around $\lambda \sim 0$ was calculated in [5–8]. Their results are expressed using the Bessel functions, which has a $\sim 1/\Sigma V$ gap from zero, reflecting the fact that no spontaneous symmetry breaking occurs at finite volumes.

Recently, an interpolation between the p and ϵ regimes was considered in [4]. The recipe for the calculation is to keep the same counting rule as in the p expansion but to integrate the zero-modes nonperturbatively like in the ϵ expansion. Partial quenching is performed with the so-called replica trick so that results at arbitrary nondegenerate set of quark masses can be compared to lattice QCD. Using this hybrid method, the results mentioned above (in the p expansion [9,10] and in the ϵ expansion [5–8]) are smoothly connected. Comparison with the lattice data is, therefore, no longer limited in either the ϵ or p regimes, and more precise determination of Σ is possible.

Here we briefly reproduce the result of [4] where we consider a general theory with N_f flavors of sea quarks. The spectral density in a fixed topological sector of Q is given by

$$\rho_Q(\lambda) = \Sigma_{\mathrm{eff}}\hat{\rho}_Q^\epsilon(\lambda\Sigma_{\mathrm{eff}}V, \{m_{\mathrm{sea}}\Sigma_{\mathrm{eff}}V\}) + \rho^p(\lambda, \{m_{\mathrm{sea}}\}), \qquad (5)$$

where two terms $\hat{\rho}_Q^\epsilon(\lambda\Sigma_{\mathrm{eff}}V, \{m_{\mathrm{sea}}\Sigma_{\mathrm{eff}}V\})$ and $\rho^p(\lambda, \{m_{\mathrm{sea}}\})$ are given in the following. Σ_{eff} includes the leading finite quark mass correction to Σ that modifies the overall normalization of the spectrum, and is therefore called the *effective* chiral condensate.

The spectrum of the near-zero modes ($\lambda \sim 1/\Sigma V$) is mainly affected by the zero-momentum pion fields. The first term in (5) has the same functional form as the one at the leading order of the ϵ expansion [5–8], which is expressed in terms of dimensionless combinations $\lambda\Sigma_{\mathrm{eff}}V$ and $\{m_{\mathrm{sea}}\Sigma_{\mathrm{eff}}V\} = \{m_1\Sigma_{\mathrm{eff}}V, \cdots, m_{N_f}\Sigma_{\mathrm{eff}}V\}$:

$$\hat{\rho}_Q^\epsilon(\zeta, \{\mu_{\mathrm{sea}}\}) \equiv C_2\frac{|\zeta|}{2\prod_f^{N_f}(\zeta^2 + \mu_f^2)}\frac{\det\tilde{\mathcal{B}}}{\det\mathcal{A}}, \qquad (6)$$

with $N_f \times N_f$ matrix $\mathcal{A}$ and $(N_f + 2) \times (N_f + 2)$ matrix $\tilde{\mathcal{B}}$ defined by $\mathcal{A}_{ij} = \mu_i^{j-1}I_{Q+j-1}(\mu_i)$ and $\tilde{\mathcal{B}}_{1j} = \zeta^{j-2}J_{Q+j-2}(\zeta)$, $\tilde{\mathcal{B}}_{2j} = \zeta^{j-1}J_{Q+j-1}(\zeta)$, $\tilde{\mathcal{B}}_{ij} = (-\mu_{i-2})^{j-1}I_{Q+j-1}(\mu_{i-2})$, $(i \neq 1, 2)$, respectively [J_k's and I_l's denote the (modified) Bessel functions.]. The phase factor C_2 is 1 for $N_f = 2$ and 3.

The second term in (5) is a logarithmic NLO correction (chiral logarithms) which is also partly seen in the conventional p expansion [10]. With the meson mass $M_{ij}^2 \equiv (m_i + m_j)\Sigma/F^2$, which is made of either sea quark (f) or valence quark (v), it is given by[1]

$$\rho^p(\lambda, \{m_{\mathrm{sea}}\}) \equiv -\frac{\Sigma}{\pi F^2}\mathrm{Re}\bigg[\sum_f^{N_f}(\bar{\Delta}(M_{fv}^2) - \bar{\Delta}(M_{ff}^2/2))$$
$$- (\bar{G}(M_{vv}^2) - \bar{G}(0))\bigg]\bigg|_{m_v=i\lambda}. \qquad (7)$$

where

---

[1] In this paper, we use simplified notations: $\bar{\Delta}(M^2)$ and $\bar{G}(M^2)$ correspond to $\bar{\Delta}(0, M^2)$ and $\bar{G}(0, M^2, M^2)$ in [4], respectively.

$$\bar{G}(M^2) = \begin{cases} \frac{1}{2}[\bar{\Delta}(M^2) + (M^2 - M_{ud}^2)\partial_{M^2}\bar{\Delta}(M^2)] & (N_f = 2), \\ \frac{1}{3}\left[-\frac{2(M_{ud}^2 - M_{ss}^2)^2}{9(M^2 - M_\eta^2)^2}\bar{\Delta}(M_\eta^2) + \left(1 + \frac{2(M_{ud}^2 - M_{ss}^2)^2}{9(M^2 - M_\eta^2)^2}\right)\bar{\Delta}(M^2) + \frac{(M^2 - M_{ud}^2)(M^2 - M_{ss}^2)}{(M^2 - M_\eta^2)}\partial_{M^2}\bar{\Delta}(M^2) \right] & (N_f = 2 + 1, 3), \end{cases} \tag{8}$$

$$\bar{\Delta}(M^2) = \frac{M^2}{16\pi^2} \ln\frac{M^2}{\mu_{\text{sub}}^2} + \bar{g}_1(M^2). \tag{9}$$

Here, the physical meson masses are given by the leading-order relations $M_{ud}^2 = 2m_u\Sigma/F^2 = 2m_d\Sigma/F^2$, $M_{ss}^2 = 2m_s\Sigma/F^2$, and $M_\eta^2 = (M_{ud}^2 + 2M_{ss}^2)/3$. The scale μ_{sub} ($= 770$ MeV in this work) is a subtraction scale.

The function given by $\bar{g}_1(M^2) = g_1(M^2) - 1/M^2V$ denotes a finite volume correction from nonzero-momentum pion modes. In the p expansion, it is expressed by the modified Bessel function K_1 [29] while in the ϵ expansion a polynomial expression is used [30]. In this study, we need the both expressions:

$$\bar{g}_1(M^2) = \begin{cases} \sum\limits_{a\neq 0, |n_i|\leq n_1^{\text{max}}} \frac{\sqrt{M^2}}{4\pi^2|a|} K_1(\sqrt{M^2}|a|) - \frac{1}{M^2V} & (|M|L > 2) \\ -\frac{M^2}{16\pi^2} \ln(M^2V^{1/2}) - \sum\limits_{n=1}^{n_2^{\text{max}}} \frac{\beta_n}{(n-1)!} M^{2(n-1)} V^{(n-2)/2} & (|M|L \leq 2) \end{cases}, \tag{10}$$

where a_μ denotes a four-vector $a_\mu = (n_1L, n_2L, n_3L, n_4T)$ with integer n_i's and β_i's are the *shape coefficients* defined in [30]. Their formula and numerical values for the first several β_n's are summarized in Appendix . In our numerical study, we truncate the sum at $n_1^{\text{max}} = 7$ and $n_2^{\text{max}} = 300$, which indeed shows a good convergence around the threshold $|M|L = 2$. We note that both $\bar{\Delta}(M^2)$ and $\bar{G}(M^2)$ are finite even in the limit of $M \to 0$.

The effective chiral condensate Σ_{eff} in (5) is given by

$$\Sigma_{\text{eff}} = \Sigma\left[1 - \frac{1}{F^2}\left(\sum_f^{N_f} \bar{\Delta}(M_{ff}^2/2) - \bar{G}(0) - 16L_6^r\sum_f^{N_f} M_{ff}^2\right)\right], \tag{11}$$

where L_6^r (renormalized at μ_{sub}) is one of the low-energy constants at NLO [2]. From the sea quark mass dependence of Σ_{eff}, one can determine Σ as well as F and L_6^r.

In the expression (5), dependence on the topological charge Q is encoded only in the first term $\Sigma_{\text{eff}}\hat{\rho}_Q^\epsilon(\lambda\Sigma_{\text{eff}}V, \{m_{\text{sea}}\Sigma_{\text{eff}}V\})$ and the second term $\rho^p(\lambda, \{m_{\text{sea}}\})$ does not depend on Q since it is a contribution from nonzero momentum modes. On the other hand, the chiral logarithm manifests itself in the both terms through $\bar{\Delta}(M^2)$. Since M^2 could also contain λ through $m_\nu = i\lambda$, the spectral density shows a nonanalytic functional form.

The above ChPT results are subject to higher-order corrections in the p expansion, for which the expansion parameter is either M^2/F^2 or $1/(FV^{1/4})^2$. Although the zero-mode contribution is treated nonperturbatively, there are 2-loop contributions of nonzero momentum modes that could also couple to the zero-mode and introduce different types of group integrals. At the 2-loop level, these contributions may have the order M^4/F^4, $M^2/(F^4V^{1/2})$, or $1/(F^4V)$, whose coefficients are unknown. We therefore need to carefully check the convergence of the expansion at NLO for our parameter sets.

In the following analysis, we test the NLO formula with various sets of quark masses, as well as different lattice volumes ($L = 16, 24$) for the $N_f = 2 + 1$ runs and different topological sectors for the $N_f = 2$ runs, in order to confirm the convergence.

III. LATTICE QCD SIMULATIONS

Numerical simulations of lattice QCD are performed with the Iwasaki gauge action [31] at $\beta = 2.3$ (except for the run of $N_f = 2$ QCD at $m_{ud} = 0.002$ for which we choose $\beta = 2.35$) including 2, $2 + 1$ (m_s fixed), and 3 ($m_{ud} = m_s$) flavors of dynamical quarks. For the quark action, we employ the overlap-Dirac operator [11]

$$D(m) = \left(m_0 + \frac{m}{2}\right) + \left(m_0 - \frac{m}{2}\right)\gamma_5\text{sgn}[H_W(-m_0)], \tag{12}$$

where m denotes the quark mass and $H_W \equiv \gamma_5 D_W(-m_0)$ is the Hermitian Wilson-Dirac operator with a large negative mass $-m_0$. We take $m_0 = 1.6$ throughout our simulations (here and in the following the parameters are given in the lattice unit). For the details of numerical implementation of the overlap-Dirac operator, we refer to our previous paper [17].

It is known that the numerical cost for the dynamical simulation of the overlap fermions becomes prohibitively large when $H_W(-m_0)$ has (near-)zero-modes. To avoid this problem, we introduce extra Wilson fermions and associated twisted-mass bosonic spinors to generate a weight

$$\frac{\det[H_W^2(-m_0)]}{\det[H_W^2(-m_0) + m_t^2]}, \tag{13}$$

in the functional integrals [21,32,33]. Both of these fermions and ghosts are unphysical as their masses are of order of the lattice cutoff, and do not affect low-energy physics. The numerator suppresses the appearance of

near-zero-modes, while the denominator cancels unwanted effects from high modes. The *twisted-mass* parameter m_t controls the value of threshold below which the eigen-modes are suppressed. In our numerical studies, we set $m_t = 0.2$.

With the determinant (13) the index of the overlap-Dirac operator, or the topological charge in the continuum limit [34], never changes from its initial value during the mo-lecular dynamics steps since its change always requires crossing zero eigenvalue of $H_W(-m_0)$. In this work the simulations are mainly performed in the trivial topological sector, $Q = 0$. In order to check the topological charge dependence, we also carry out independent simulations at $Q = +1, -2$, and -4 at several sets of parameters.

Simulation parameters are summarized in Table I. The lattice size is $V = 16^3 \times 32$ for the $N_f = 2$ runs, while it is $V = 16^3 \times 48$ for the main $N_f = 2 + 1$ and $N_f = 3$ runs. In order to investigate the finite-volume scaling, we also simulate on a $24^3 \times 48$ lattice at the same lattice spacing with two choices of sea quark masses $(m_{ud}, m_s) = (0.015, 0.080)$ and $(0.025, 0.080)$. For the de-termination of the lattice spacing $a = 0.11$–0.12 fm

$(a^{-1} = 1.7$–1.8 GeV$)$, we choose the Ω-baryon mass as the input for the $N_f = 2 + 1$ and 3 ensembles [35], while it is determined from the heavy quark potential with an input $r_0 = 0.49$ fm for the $N_f = 2$ case. Our lattice size is then estimated as $L \sim 1.8$ fm for the $N_f = 2 + 1$ runs, and $L \sim 1.9$ fm for the $N_f = 2$ runs.

In the $N_f = 2$ runs, seven different values of the up and down quark mass m_{ud} are taken. For the $N_f = 2 + 1$ runs, we choose two different values of strange quark mass m_s $(= 0.080$ and $0.100)$ and six (for the former) or five (for the latter) values of m_{ud} are chosen. For the degenerate $N_f = 3$ flavor runs, we take four different values of $m_{ud} = m_s$. Note that the lightest up and down quark mass $m_{ud} = 0.002$ in the $N_f = 2$ or $N_f = 2 + 1$ ensem-bles roughly correspond to 3 MeV in the physical unit, with which pions are in the ϵ regime while kaons still remain in the p regime.

We compute 50–80 pairs of low-lying eigenvalues (that we denote λ^{ov}'s) of the massless overlap-Dirac operator $D(0)$ at every 5 or 10 (depending on the parame-ters) trajectories. In the calculation of the eigenvalues, we employ the implicitly restarted Lanczos algorithm

TABLE I. Summary of lattice parameters. For the 2-, 2 + 1-, and 3-flavor runs, the values of β, a^{-1}, (m_{ud}, m_s) and Q are listed. Other parameters are those for the HMC simulations: N_{trj} denotes the number of trajectory, τ_{trj} is the unit trajectory length, and N_{auto} denotes the integrated autocorrelation length (number of trajectories) of the lowest eigenvalue.

N_f	V	β	a^{-1}(GeV)	m_{ud}	m_s	Q	N_{trj}	τ_{trj}	N_{auto}
2	$16^3 \times 32$	2.35	1.776(38)	0.002	∞	0	4680	0.5	34(12)
		2.30	1.667(17)	0.015	∞	0	10 000	0.5	48(21)
				0.025	∞	0	10 000	0.5	38(16)
				0.035	∞	0	10 000	0.5	28(12)
				0.050	∞	0	10 000	0.5	24(9)
				0.050	∞	-2	5000	0.5	50(24)
				0.050	∞	-4	5000	0.5	34(16)
				0.070	∞	0	10 000	0.5	23(10)
				0.100	∞	0	10000	0.5	9(3)
2 + 1	$16^3 \times 48$	2.30	1.759(10)	0.002	0.080	0	5000	0.5	17(9)
				0.015	0.080	0	2500	1.0	15(6)
				0.015	0.080	1	1800	1.0	5(1)
				0.025	0.080	0	2500	1.0	11(5)
				0.035	0.080	0	2500	1.0	24(11)
				0.050	0.080	0	2500	1.0	9(5)
				0.015	0.100	0	2500	1.0	5(3)
				0.025	0.100	0	2500	1.0	10(3)
				0.035	0.100	0	2500	1.0	34(21)
				0.050	0.100	0	2500	1.0	5(3)
	$24^3 \times 48$	2.30	1.759(10)	0.015	0.080	0	2500	1.0	2(1)
				0.025	0.080	0	2500	1.0	3(2)
3	$16^3 \times 48$	2.30	1.759(10)	0.025	0.025	0	2500	1.0	4(1)
				0.035	0.035	0	2500	1.0	5(1)
				0.080	0.080	0	2500	1.0	20(12)
				0.100	0.100	0	2500	1.0	24(15)

for the chirally projected operator $P_+ D(0) P_+$ (where $P_+ = (1 + \gamma_5)/2$) of which eigenvalue corresponds to $\mathrm{Re}\lambda^{ov}$. From each eigenvalue of $P_+ D(0) P_+$, the eigenvalue λ^{ov}, as well as its complex conjugate, are extracted through the relation $|1 - \lambda^{ov}/m_0|^2 = 1$. In order to compare with ChPT, every complex eigenvalue λ^{ov} is mapped onto the imaginary axis as $\lambda \equiv \mathrm{Im}\lambda^{ov}/(1 - \mathrm{Re}\lambda^{ov}/(2m_0))$. The difference between λ and $\mathrm{Im}\lambda^{ov}$ is a discretization effect, which is negligible (within 1%) for $|\lambda^{ov}| < 0.03$. In the analysis, we consider positive λ only.

For each run, 1800–10 000 (depending on the parameters) trajectories are accumulated using the hybrid Monte Carlo algorithm. The integrated autocorrelation time N_{auto} of the lowest λ in the unit of the trajectory length τ_{trj} is also listed in Table I. Because of its infrared nature, the lowest Dirac eigenvalue is expected to be most difficult to decorrelate and thus has the longest autocorrelation time. The measurement is not stable and the statistical error is as large as 50% in some cases, but N_{auto} is typically $O(50)$ or less. In the following analysis, the statistical error for the spectral density and other quantities is estimated by the jackknife method after binning the data in every 100 trajectories.

Details of configuration generation and other quantities will be reported in a separate paper.

IV. EXTRACTION OF LECS AT EACH SET OF SEA QUARK MASSES

Although a global fit of the lattice data for spectral density to the NLO ChPT formula is possible in principle, we prefer to simplify the analysis, for better understanding of numerical sensitivity of the lattice data and the errors in the final result. We first consider the mode number below λ, or the integrated eigenvalue density,

$$N_Q(\lambda) \equiv V \int_0^\lambda d\lambda' \rho_Q(\lambda'), \qquad (14)$$

at each set of sea quark masses. The analytic ChPT result (5) is also integrated numerically from 0 to λ. In the second term of (5) we can replace Σ/F^2 by $\Sigma_{\mathrm{eff}}/F^2$ as their difference is a higher-order effect. Then, there are two unknown parameters in the formula: Σ_{eff} and F.

The data points of $N_Q(\lambda)$ at two reference values of λ are hence sufficient to determine the parameters. We take $\lambda = 0.004$ (~ 7 MeV) and 0.017 (~ 30 MeV) as the two reference points, except for the case with $m_{ud} = 0.002$, for which we choose $\lambda = 0.0125$ and 0.017 ($N_f = 2$) or 0.010 and 0.017 ($N_f = 2 + 1$). For the $Q \neq 0$ runs we take $\lambda = 0.01$ and 0.02. Effectively, the lower λ point determines Σ_{eff}, while the other point is more sensitive to the NLO

TABLE II. Extracted values of Σ_{eff} and F using $N_f = 3$ and $N_f = 2$ ChPT.

N_f (lattice)	m_{ud}	m_s	$N_f = 3$ ChPT		(reduced) $N_f = 2$ ChPT		comment
			Σ_{eff}	F	Σ_{eff}	F	
2	0.002	∞	$\cdots$	$\cdots$	0.002 18(19)	0.059(65)	($\beta = 2.35$)
	0.015	∞	$\cdots$	$\cdots$	0.003 62(15)	0.0527(20)	
	0.025	∞	$\cdots$	$\cdots$	0.003 53(15)	0.0664(90)	
	0.035	∞	$\cdots$	$\cdots$	0.003 82(14)	0.0681(64)	
	0.050	∞	$\cdots$	$\cdots$	0.004 49(15)	0.0644(20)	
	0.050	∞	$\cdots$	$\cdots$	0.004 00(16)	0.0728(60)	($Q = -2$)
	0.050	∞	$\cdots$	$\cdots$	0.004 82(19)	0.0636(19)	($Q = -4$)
	0.070	∞	$\cdots$	$\cdots$	0.004 80(15)	0.0707(23)	
	0.100	∞	$\cdots$	$\cdots$	0.004 78(12)	0.0862(72)	
2 + 1	0.002	0.080	0.002 04(07)	0.0469(102)	0.002 04(05)	0.0425(49)	
	0.015	0.080	0.003 14(18)	0.0536(15)	0.003 05(17)	0.0551(16)	
	0.015	0.080	0.003 54(48)	0.0521(25)	0.003 19(58)	0.0558(62)	($Q = 1$)
	0.015	0.080	0.002 73(06)	0.0520(25)	0.002 70(06)	0.0545(26)	($L = 24$)
	0.025	0.080	0.003 33(18)	0.0624(20)	0.003 26(18)	0.0647(20)	
	0.025	0.080	0.002 99(06)	0.0600(23)	0.002 97(05)	0.0629(24)	($L = 24$)
	0.035	0.080	0.004 04(39)	0.0636(17)	0.003 93(36)	0.0666(16)	
	0.050	0.080	0.004 23(22)	0.0696(16)	0.004 13(21)	0.0738(16)	
	0.015	0.100	0.003 09(14)	0.0564(19)	0.003 03(13)	0.0578(19)	
	0.025	0.100	0.003 49(20)	0.0622(17)	0.003 42(19)	0.0642(17)	
	0.035	0.100	0.004 18(40)	0.0647(14)	0.004 09(38)	0.0673(14)	
	0.050	0.100	0.003 83(13)	0.0713(16)	0.003 76(13)	0.0747(16)	
3	0.025	0.025	0.003 35(23)	0.0531(10)	$\cdots$	$\cdots$	
	0.035	0.035	0.003 34(21)	0.0612(24)	$\cdots$	$\cdots$	
	0.080	0.080	0.004 53(23)	0.0767(14)	$\cdots$	$\cdots$	
	0.100	0.100	0.005 20(22)	0.0835(22)	$\cdots$	$\cdots$	

effects that contain $1/F^2$. We check that the resulting values of Σ_{eff} and F are stable against the change of the reference points by varying them by a factor of 2 or 3 while keeping the higher point less than 0.030 to avoid possible higher-order corrections. The reference points are different for the ϵ regime runs and for the $Q \neq 0$ runs, because the small eigenvalues are highly suppressed (the lowest eigenvalue is larger than 0.004) for these cases.

For the $N_f = 2 + 1$ lattice data, we test both the $N_f = 2 + 1$ and $N_f = 2$ ChPT formulas. For the latter case, the strange quark is assumed to be decoupled from the theory, which we call *reduced $N_f = 2$ ChPT*.

Numerical results are listed in Table II. Before moving to further analysis of the results let us describe our observations for the spectral function.

Figures. 1–8 show the spectral density and its integral (14) obtained in our lattice simulations. A typical example is that for $N_f = 2 + 1$ QCD in the p regime (Fig. 1).
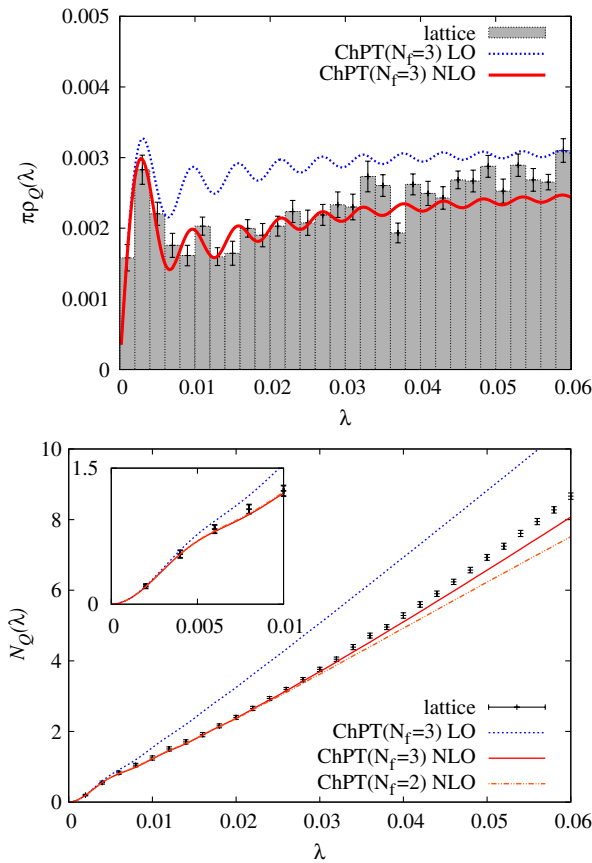
FIG. 1 (color online). $N_f = 2 + 1$ lattice QCD results for the spectral density $\rho_Q(\lambda)$ (top panel) and the mode number $N_Q(\lambda)$ (bottom panel) of the Dirac operator at $m_{ud} = 0.015$, $m_s = 0.080$, and $Q = 0$. The lattice data [histogram (top) or solid symbols (bottom)] are compared with the NLO ChPT formula drawn by solid curves. For comparison, the prediction of the leading-order ϵ expansion (dotted curves) and that of the NLO formula but with $N_f = 2$ flavors (dashed curve) are also shown.
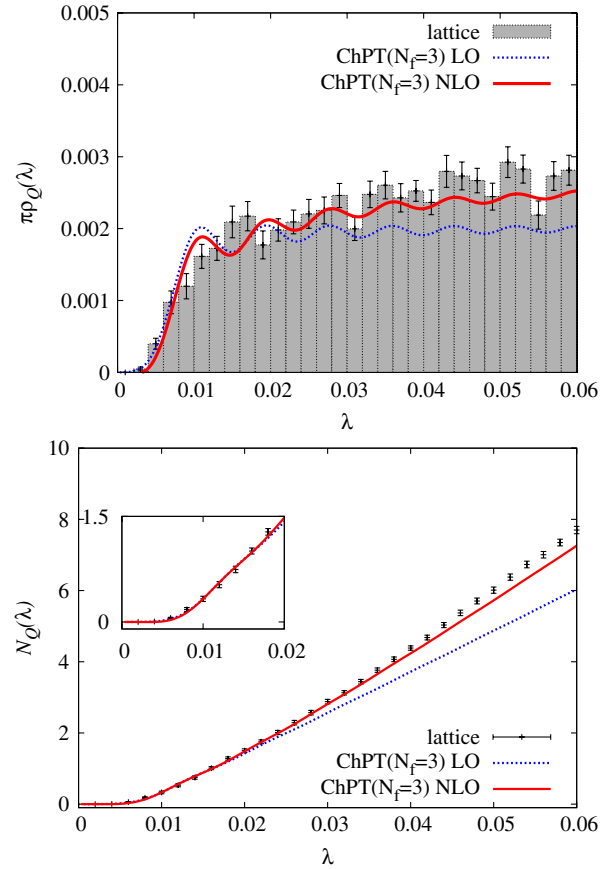

FIG. 2 (color online).   Same as Fig. 1, but at $m_{ud} = 0.002$ and $m_s = 0.080$.

The upper panel shows the histogram plot of the spectral function $\rho_Q(\lambda)$ as a function of λ. The lattice data for each bin have a jackknife estimate of the statistical error. The solid (red) curve represents the NLO ChPT formula, while the dotted (blue) curve corresponds to the leading-order result (in the ϵ expansion). Since the first reference point is 0.004, it probes the first peak, which corresponds to the lowest eigenvalue. Starting from the second peak, the effect of the NLO term appears, as clearly seen from the difference of the two curves. Therefore, by taking the second reference point at 0.017, the data have enough sensitivity to the NLO parameter $1/F^2$. This observation is of course specific to the particular volume of our lattice; on larger lattices, the peaks move toward the origin and the impact of the NLO term would become less significant on the second or third peaks (see Fig. 8).

The agreement with the formula can be seen more clearly by looking at $N_Q(\lambda)$, the mode number below λ (lower panel). The lattice data depart from the leading-order curve (dotted), which corresponds to the first term $\Sigma_{\text{eff}}\hat{\rho}_Q^\epsilon$ in (5), at around 0.005 (see the inset). Then, the data follow the nontrivial functional form of the NLO formula (solid), which comes from the chiral logarithm originating from pion loops. The NLO formula works precisely up to
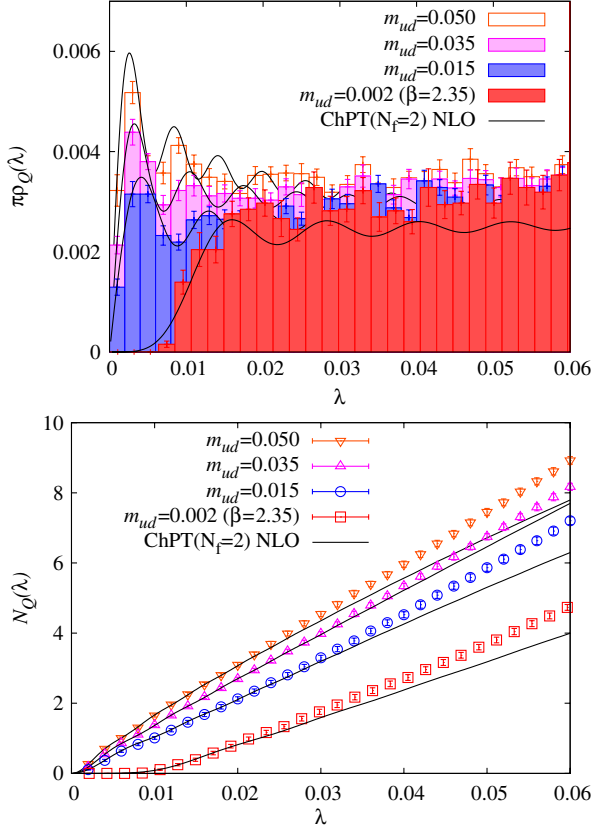
FIG. 3 (color online). $N_f = 2$ lattice QCD results for the spectral density $\rho_Q(\lambda)$ (top panel) and the mode number $N_Q(\lambda)$ (bottom panel) of the Dirac operator at various sea quark masses. The global topological charge is fixed to zero. The NLO ChPT ($N_f = 2$) results are drawn by solid curves. Note that the $\beta = 2.35$ data are rescaled as $\lambda \to 1.065\lambda$ and $\rho \to 1.209\rho$ according to the difference of the lattice spacing a.

FIG. 4 (color online). Same as Fig. 3 but for the $N_f = 2 + 1$ data at $m_s = 0.080$. Solid curves show the NLO ChPT ($N_f = 3$) formula.

$\lambda \sim 0.025$, and the deviation is still within two sigma at $\lambda \sim 0.04$, which is about the half of the physical strange quark mass m_s^{phys}. This is a typical range where the NLO ChPT is valid, and the higher-order corrections would become sizable above this value. In contrast to a recent work by Giusti and Lüscher [36], where they take a wider range of λ (up to $\lambda \sim 95$ MeV) into the analysis, we conservatively choose the reference points below 30 MeV, so that (partially quenched) ChPT with an imaginary valence quark mass $i\lambda$ can be safely applied.

In Fig. 1, the difference between the $N_f = 3$ and $N_f = 2$ (dashed curve) formulas is not sizable below $\lambda \sim$ 0.03–0.04. This is natural because the strange quark (with $m_s = 0.08$) decouples from the dynamics of the low-lying modes. As a result, the extraction of Σ_{eff} does not significantly depend on the formula we use ($N_f = 3$ or $N_f = 2$).

The convergence of the chiral expansion is better in the ϵ regime as shown in Fig. 2, in which the $N_f = 2 + 1$ lattice data at $m_{ud} = 0.002$ and $m_s = 0.080$ are plotted. In the plot of the mode number (lower panel), the LO and NLO
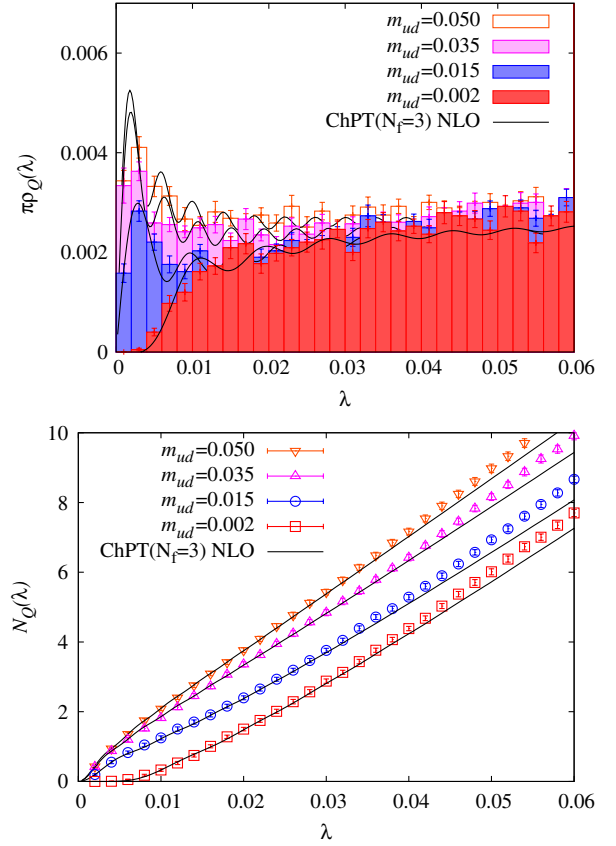
curves coincide up to $\lambda \sim 0.025$. Beyond this value, we observe some deviation, which is also seen in the histogram plot (upper panel).

The NLO ChPT correction in this work explains the disagreement of the lattice data with the expectation from the random matrix theory found in our previous work [15,16]. Namely, if we adjust the parameter Σ_{eff} using the lowest eigenvalue distribution (the first peak of the histogram), then the second peak would not agree at the leading order. Indeed, the NLO contribution is responsible for this.

V. SCALING TESTS WITH VARIOUS PARAMETERS

A. Sea quark masses

Figs. 3 and 4 compare the spectral density and its integral at various sea quark masses. The data are obtained for $N_f = 2$ (Fig. 3) and $N_f = 2 + 1$ (Fig. 4) with up and down quark masses in the p regime ($m_{ud} = 0.050, 0.035, 0.015$) and in the ϵ regime ($m_{ud} = 0.002$). Note that the β value of the ϵ regime run in $N_f = 2$ QCD is slightly higher ($\beta = 2.35$) than in other runs ($\beta = 2.30$).

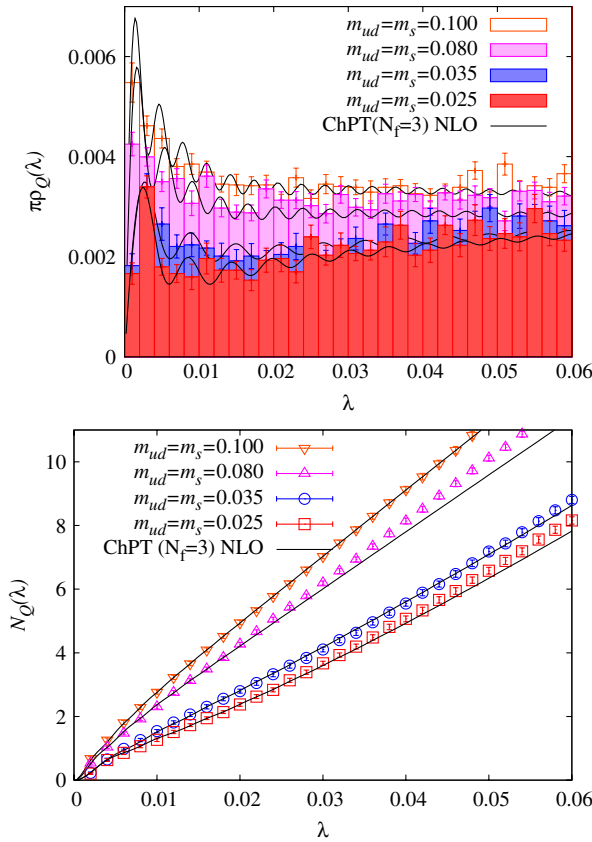FIG. 5 (color online). Same as Fig. 4 but for degenerate $N_f = 3$ data.

FIG. 6 (color online). Dependence on the topological charge of the $N_f = 2$ lattice QCD results at $m_{ud} = 0.050$. For the ChPT curves (solid), the same input values of Σ_{eff}, F determined from $Q = 0$ are used.

In the plot, we adjust the value of λ by a factor of 1.065 which corresponds to the ratio of lattice spacings between the two β values.

In the plots, we clearly observe the sea quark mass dependence. For heavier sea quarks, the spectral density shows a higher peak near the lowest eigenvalue (around $\lambda \sim 0.004$), and the peak height becomes lower by reducing the quark mass. As one enters the ϵ regime, the lowest eigenvalue is pushed up to $\lambda \sim 0.015$. This is what we expect for the effect of the fermionic determinant $\prod_k (\lambda_k^2 + m_{ud}^2)^2$. Namely, when the quark mass is reduced to the value around (or below) the lowest eigenvalue, those eigenvalues are suppressed.

The expectation from NLO ChPT precisely follows the lattice data (solid curves in Figs. 3 and 4). Here the values of Σ_{eff} and F are determined for each set of sea quark mass, so that the comparison is not parameter-free. But, still the precise agreement of the shape of the spectral density is encouraging. We investigate the mass dependence of Σ_{eff} in the next section.

In Fig. 5, similar plots are also shown for the $N_f = 3$ lattice data where three sea quarks have a degenerate mass ($m_{ud} = m_s$). We have four values of the quark mass (0.100, 0.080, 0.035, and 0.025) in the p regime. In $N_f = 3$ QCD, we observe a stronger dependence on the quark mass than
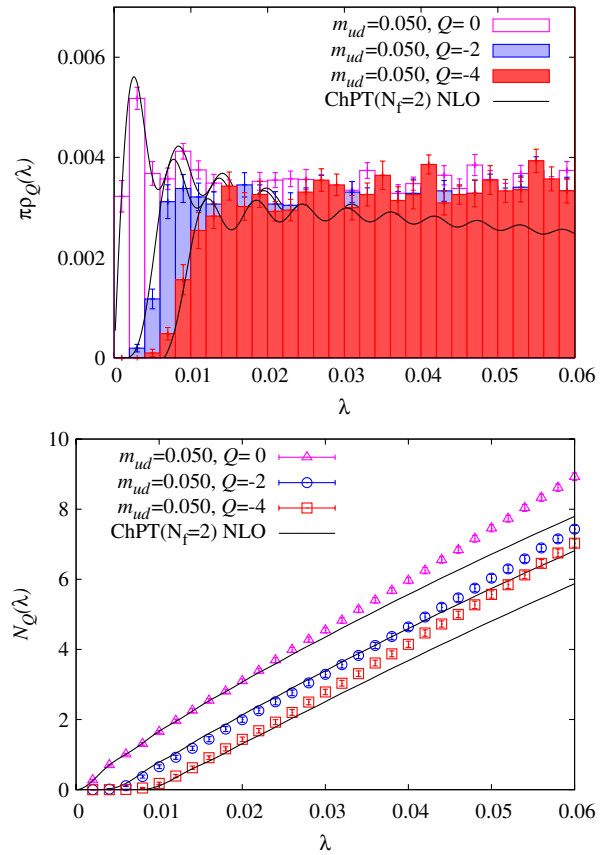
in $N_f = 2$ or $2 + 1$, as suggested by the NLO formula for Σ_{eff} in (11).

B. Topological charge

In the low-eigenvalue region, the Dirac spectral density is known to be sensitive to the topological charge Q of the gauge fields, which is clearly seen in Figs. 6 and 7. The solid curves in the plots show the expectation from the NLO ChPT with input parameters determined from the $Q = 0$ lattice data. Therefore, there is no free parameter to be adjusted in the curves for the $Q \neq 0$ cases. We observe that the Q dependence of the lattice data is qualitatively well described by ChPT.

Note, however, that the extracted values of Σ_{eff} and F from $Q \neq 0$ data show a 2.2σ difference for $N_f = 2$ while they are consistent in the $N_f = 2 + 1$ case. Since the topological charge dependence is a part of finite volume effects [37–39], which should be accounted for by the effective theory analysis, the deviation suggests possible higher-order effects in the $1/L$ expansion of ChPT. Indeed, the $N_f = 2$ runs are carried out with a shorter temporal extent $T = 32$ than that of $N_f = 3$ ($T = 48$), so that the lattice volume is $\sim 17\%$ smaller in the physical unit.
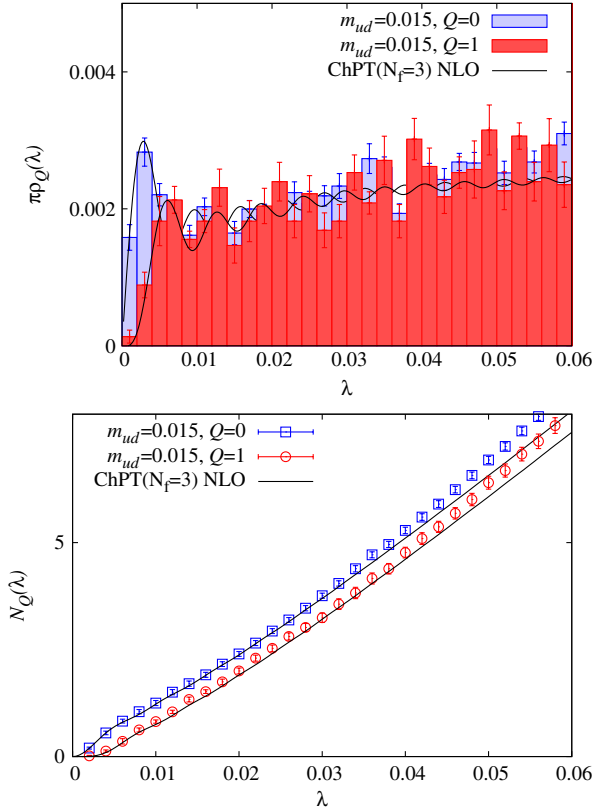
FIG. 7 (color online).   Same as Fig. 6 but for $N_f = 2 + 1$ QCD at $m_{ud} = 0.015$ and $m_s = 0.080$.

FIG. 8 (color online).   Spectral density (top) and the mode number (bottom) on the larger volume lattice ($L = 24$ [~ 2.7 fm]) at $m_{ud} = 0.015$ and 0.025 with a fixed value of $m_s = 0.080$. For comparison, $L = 16$ lattice results as well as the ChPT predictions (solid curves) are shown in the bottom panel where the same input values of Σ_{eff}, F (from $L = 24$ results) are used.

Higher-order finite volume effects may therefore be enhanced for $N_f = 2$. In the final results of the $N_f = 2$ data, we add this $\sim 11\%$ deviation as an estimate of the systematic error due to the finite volume.

C. Finite volume

The finite volume scaling can be tested more explicitly with the $N_f = 2 + 1$ runs, for which the $L = 24 (\sim 2.7$ fm) lattice data are available. Here we note that the comparison of Σ_{eff} obtained on the $L = 16$ and $L = 24$ lattices is not straightforward, because there is a finite volume effect encoded in $\bar{g}_1(M^2)$ in the definition of Σ_{eff} (11). It is still possible to analytically convert the values of $\bar{g}_1(M^2)$ in different volumes. The results for Σ_{eff} obtained on the $L = 24$ lattice are converted to those at the smaller volume as $\Sigma_{\mathrm{eff}} = 0.002\,73(06) \rightarrow 0.003\,05(15)$ at $m_{ud} = 0.015$ and $\Sigma_{\mathrm{eff}} = 0.002\,99(06) \rightarrow 0.003\,36(12)$ at $m_{ud} = 0.025$, which agrees with the values calculated on the $L = 16$ lattice: $\Sigma_{\mathrm{eff}} = 0.003\,14(18)$ and $0.003\,33(18)$, respectively. In fact, as shown in Fig. 8, we find that the same inputs of (converted) Σ_{eff} and F describe the data at different volumes very well.

From these analyses, the systematic error due to finite volume is estimated as $\sim 3\%$, which is taken from the difference between the $L = 16$ and $L = 24$ (after the conversion) results.
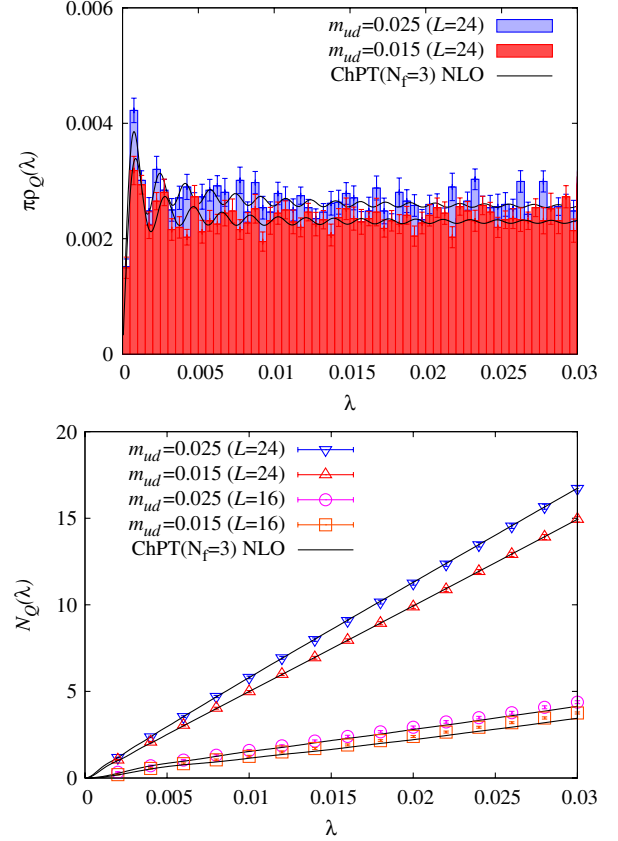
VI. DETERMINATION OF THE CHIRAL CONDENSATE

The extracted values of Σ_{eff} and F for each lattice ensemble are summarized in Table II. Note that Σ_{eff} is extracted at the NLO accuracy, while the value of F which first appears in the NLO term might receive larger systematic corrections from the NNLO contributions.

As already noted above, since m_s is fixed at a large value (0.080 or 0.100) in the $N_f = 2 + 1$ ensembles, there is little difference between the reduced $N_f = 2$ and $N_f = 2 + 1$ ChPT analysis near the chiral limit of m_{ud}: Σ_{eff} and F are almost equal within the statistical errors. The difference between $m_s = 0.080$ and $m_s = 0.100$ is also small (always less than 1σ), and therefore we concentrate on the data at $m_s = 0.080$ in the following.

Now we analyze the sea quark mass dependence of Σ_{eff}. The NLO formula for Σ_{eff} (11) contains the low-energy constants Σ, F, and L_6 as parameters. The chiral condensate Σ, in particular, appears at the leading order, and its determination through the quark mass dependence of Σ_{eff}
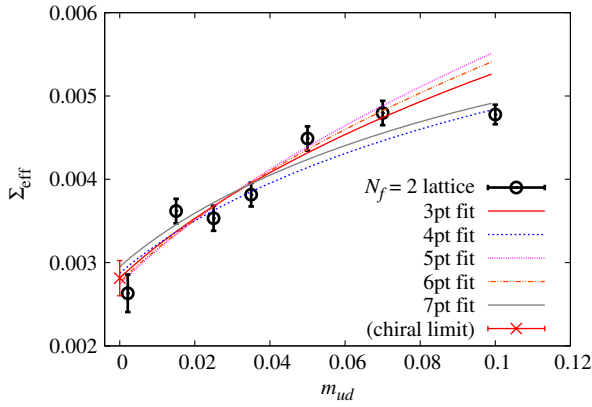
FIG. 9 (color online).   Chiral extrapolation of Σ_{eff} in $N_f = 2$ QCD. The data point in the ϵ regime ($m_{ud} = 0.002$) is rescaled to absorb the small difference of the lattice spacing. The two-parameter fits with an input $F = 0.0474$ [40] for various number of data points included in the fit are drawn together with the lattice data points (open circles). The chiral limit is that for the 3-point fit.

is valid at the NLO accuracy, while the other parameters controlling the NLO correction can be determined at the leading order.

In the fit of the lattice data, we attempt two procedures: a 3-parameter (Σ, F, L_6) fit without any additional inputs, and 2-parameter (Σ, L_6) fits for several input values of F. In the 2-parameter fits, the value of F determined in our previous works both in the p regime ($F = 0.0474(30)$) [40] and in the ϵ regime ($F = 0.0524(34)$) [41] are used for the $N_f = 2$ lattice ensembles. Any difference due to the different input values of F suggests some systematic error

(although it turns out to be only $\sim 1.1\sigma$ in the final result). For the $N_f = 2 + 1$ and 3 runs, we use a naive (linear) chiral limit of F given in Table II, of which values are $F = 0.0411$ for $N_f = 3$ ChPT and $F = 0.0406$ for reduced $N_f = 2$ ChPT, respectively.

The chiral extrapolation of Σ_{eff} in $N_f = 2$ QCD is shown in Fig. 9. From the plot, we can see the crucial role played by the data point at $m_{ud} = 0.002$ which is in the ϵ regime. Without this data point, one may naively expect that the data do not have enough sensitivity to probe the curvature due to the chiral logarithm and the chiral extrapolation favors a larger value of Σ (~ 0.0032). Taking the ϵ regime data into account, the presence of chiral logarithm is consistent with the negative curvature seen in the data.

The extracted values of the LECs in $N_f = 2$ ChPT are summarized in Table III. We attempt the 2-parameter fits of various number of data points, 3–7, taken from the lowest quark mass and the 3-parameter fits with 4–7 data points. In the table, the range of m_{ud} used in the fit is listed. For the 2-parameter fits, we take two input values of F. The quality of the fits can be inferred from the value of $\chi^2/\mathrm{d.o.f.}$ also listed in the table.

As far as the heaviest point is discarded in the fits, the resulting value of Σ is insensitive to the input value of F, and it is consistent with the three-parameter fit as well. On the other hand, the determination of L_6^r is unstable, but all the data suggest $|L_6^r| < 0.001$. We take $\Sigma = 0.002\,46(15)$ and $L_6^r = -0.000\,09(13)$ as the central values, which are from the 4-point fit with the input $F = 0.0474$. For the final results of this paper, we take the deviation from the other

TABLE III. $N_f = 2$ lattice results for Σ, F, and $L_6^r(\mu_{\mathrm{sub}} = 770$ MeV$)$ extracted comparing with the $N_f = 2$ ChPT formula. The results for 2- and 3-parameter fits are listed. The values in the parenthesis $[\cdots]$ are used as an input of the chiral fit.

| m_{ud} fit range | $N_f = 2$ ChPT LECs | | | $\chi^2/\mathrm{d.o.f.}$ |
	Σ	F	L_6^r	
2 prm fit	($F = 0.0474$)			
0.002–0.025	0.002 43(18)	[0.0474]	−0.000 04(21)	4.8
0.002–0.035	0.002 46(15)	[0.0474]	−0.000 09(13)	2.5
0.002–0.050	0.002 33(12)	[0.0474]	0.000 07(10)	2.4
0.002–0.070	0.002 33(09)	[0.0474]	0.000 06(07)	1.8
0.002–0.100	0.002 46(07)	[0.0474]	−0.000 04(03)	2.4
2 prm fit	($F = 0.0524$)			
0.002–0.025	0.002 50(19)	[0.0524]	0.000 12(30)	5.2
0.002–0.035	0.002 55(15)	[0.0524]	0.000 02(18)	2.7
0.002–0.050	0.002 43(12)	[0.0524]	0.000 21(14)	2.4
0.002–0.070	0.002 46(10)	[0.0524]	0.000 18(09)	1.8
0.002–0.100	0.002 62(08)	[0.0524]	0.000 01(04)	2.8
3 prm fit				
0.002–0.035	0.001 74(45)	0.0290(71)	−0.000 24(03)	2.5
0.002–0.050	0.002 46(68)	0.0547(78)	0.000 38(90)	3.5
0.002–0.070	0.002 37(38)	0.0489(15)	0.000 09(35)	2.4
0.002–0.100	0.002 06(26)	0.0386(48)	−0.000 09(02)	2.3
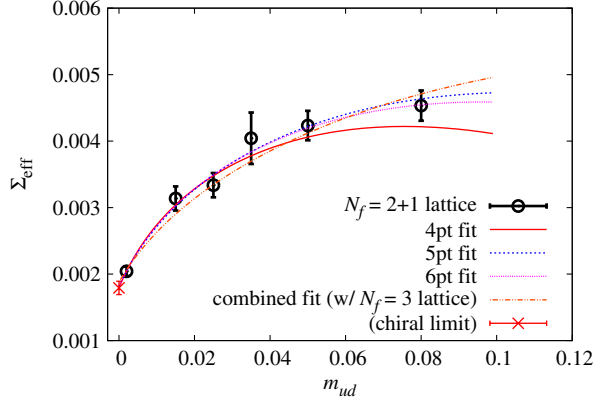
FIG. 10 (color online).   Same as Fig. 9 but for $N_f = 2 + 1$ QCD. The fit curve corresponds to that of the 3-parameter fit.

input value of F, as well as the other fitting ranges, as a systematic error due to the chiral extrapolation.

For the $N_f = 2 + 1$ lattice data, the chiral extrapolation is more stable because of the precise data point in the ϵ regime, which is simply due to higher statistics we accumulated. Figure 10 clearly shows the logarithmic curvature. Namely, a naive linear extrapolation of four data

points in the p regime ($m_{ud} = 0.015$–0.050) would lead to ~ 0.0028 in the chiral limit, while the ϵ regime point is lower (~ 0.0020).

We analyze the $N_f = 2 + 1$ lattice data listed in Table II using the 2- and 3-parameter fits. We consistently use the $N_f = 3$ formula for the data obtained with $N_f = 3$ ChPT (fourth column in Table II). The same applies for the reduced $N_f = 2$ ChPT analysis. The fit results are presented in Table IV and in Table V. The curves in Fig. 10 represent the $N_f = 3$ fits for various numbers of data points. We find that all the curves go through the data points except for the heaviest one. The chiral limit, shown by a cross symbol, is almost unchanged by taking different fit schemes (2-parameter or 3-parameter) and the number of data points included in the fit (4, 5, or 6). This is because the precise ϵ regime point works as an anchor near the chiral limit.

For $N_f = 3$ ChPT, Σ^{phys} listed in Table IV denotes the value of Σ_{eff} in the limit of $m_{ud} \to 0$ and $V \to \infty$ with a fixed strange quark mass $m_s = 0.080$. This corresponds to the *physical* value of the chiral condensate $-\langle \bar{u}u \rangle = -\langle \bar{d}d \rangle$ defined in the limit of vanishing up and down quark masses.

TABLE IV. $N_f = 2 + 1$ lattice results for Σ, F, and $L_6(\mu_{\text{sub}} = 770 \text{ MeV})$ extracted using the $N_f = 3$ ChPT formula. The results for 2- and 3-parameter fits are listed. The values with parenthesis $[\cdots]$ are used as an input for the chiral fit. Σ^{phys} denotes the $m_{ud} = 0$ and $V = \infty$ limit of Σ_{eff} with $m_s = 0.080$ fixed.

	$N_f = 3$ ChPT LECs			
m_{ud} fit range	Σ^{phys}	F	L_6^r	χ^2/d.o.f.
2 prm fit				
0.002–0.025	0.001 86(09)	[0.0411]	−0.000 13(09)	1.0
0.002–0.035	0.001 86(09)	[0.0411]	−0.000 14(08)	0.6
0.002–0.050	0.001 86(09)	[0.0411]	−0.000 14(07)	0.5
0.002–0.080	0.001 85(08)	[0.0411]	−0.000 14(07)	0.4
3 prm fit				
0.002–0.035	0.001 85(10)	0.0433(13)	−0.000 23(53)	1.3
0.002–0.050	0.001 86(09)	0.0406(05)	−0.000 12(25)	0.7
0.002–0.080	0.001 86(08)	0.0413(02)	−0.000 15(09)	0.5

TABLE V.   Same as Table IV but extracted using reduced $N_f = 2$ ChPT.

	reduced $N_f = 2$ ChPT LECs			
m_{ud} fit range	Σ	F	L_6^r	χ^2/d.o.f.
2 prm fit				
0.002–0.025	0.001 99(06)	[0.0406]	−0.000 44(10)	0.9
0.002–0.035	0.001 97(06)	[0.0406]	−0.000 40(09)	0.7
0.002–0.050	0.001 97(05)	[0.0406]	−0.000 39(06)	0.4
0.002–0.080	0.001 98(05)	[0.0406]	−0.000 42(04)	0.5
3 prm fit				
0.002–0.035	0.001 97(09)	0.0407(10)	−0.00042(51)	1.3
0.002–0.050	0.001 98(07)	0.0416(05)	−0.00038(21)	0.6
0.002–0.080	0.001 96(07)	0.0399(03)	−0.00044(07)	0.5

TABLE VI. The degenerate $N_f = 3$ lattice results for the LECs of $N_f = 3$ ChPT. Here, Σ denotes the chiral condensate at the limit $m_{ud} = m_s = 0$ while Σ^{phys} is the one with $m_s = 0.080$ fixed.

m_{ud}, m_s fit range	$N_f = 3$ ChPT LECs				$\chi^2/\text{d.o.f.}$
	Σ	Σ^{phys}	F	L_6^r	
2 prm fit					
0.025–0.100	0.001 52(11)	0.002 04(04)	[0.0431]	0.000 10(10)	3.1
0.025–0.100	0.001 82(14)	0.002 42(06)	[0.0531]	0.000 31(17)	2.8
3 prm fit	(combined with $N_f = 2 + 1$ data)				
0.002–0.100	0.001 45(12)	0.001 91(08)	0.0401(17)	0.000 03(7)	1.7

From Tables IV and V, we can see that results for Σ^{phys} obtained via $N_f = 2 + 1$ and reduced $N_f = 2$ ChPT formulas are consistent with each other. (We assume that Σ^{phys} in the $N_f = 2 + 1$ theory corresponds to Σ in reduced $N_f = 2$ ChPT.) The result is also stable against the changes of the number of fitting parameters and the fitting range. For the other parameters, F and L_6^r, we find larger dependence on the choice of fit procedures, which is expected because they only appear in the NLO terms.

We take $\Sigma^{\text{phys}} = 0.001 86(09)$, $F = 0.0406(05)$, and $L_6^r = -0.000 12(25)$ as the central values, which are obtained from the 5-point fit with three free parameters in $N_f = 3$ ChPT. As mentioned above, the other results are used to estimate systematic errors.

For the degenerate ($m_{ud} = m_s$) $N_f = 3$ lattice results, the number of data points is limited to four. The 3-parameter fit, therefore, does not work and we restrict ourselves to the 2-parameter fit. We attempt the fit with two values of F, 0.0431 and 0.0531, as the input. The former value is an $N_f = 3$ chiral limit of F in Table II taken with a linear function in the quark mass and the latter is the one at the lightest sea quark mass $m_{ud} = m_s = 0.025$. Because of the lack of the ϵ regime data point, the chiral limit is not as stable as in the $N_f = 2$ or $N_f = 2 + 1$ data. In fact, the resulting value of Σ strongly depends on the input value of F. Between the two representative values of F, Σ changes about 20%. Since F controls the NLO effects as seen in (11), this change suggests that the 1-loop calculation is not sufficient to control the $m_{ud} = m_s$ dependence.

We also attempt a combined fit of all the $N_f = 2 + 1$ and $N_f = 3$ data points using the $N_f = 3$ ChPT formula. The total 9 data points are simultaneously fitted with a reasonable $\chi^2/\text{d.o.f.}$ ($\simeq 1.7$). The result is given in Table VI and plotted in Figs. 10 and 11 which indicate a strong effect of chiral logarithm in the $N_f = 3$ data compared to the case of $N_f = 2$ shown in Fig. 9. The chiral limit is less than half of the value at the lowest p regime point ($m_{ud} = m_s = 0.025$). One should note, however, that the data points in the fit includes those with $m_s = 0.080$ and 0.100 which are out of the typical convergence region

of chiral expansion $m_i < m_s^{\text{phys}}/2$, so that the result may contain large systematic effects.

It is still remarkable that all the results suggest that the chiral condensate Σ of $N_f = 3$ QCD is smaller than Σ^{phys} of $N_f = 2 + 1$ or Σ of $N_f = 2$ QCD. This is consistent with the view that the chiral condensate decreases and eventually disappears as the number of flavor increases and the asymptotic freedom is lost. We take $\Sigma = 0.001 45(12)$, $F = 0.0401(17)$, and $L_6^r = 0.000 03(7)$ determined from the combined fit as the central values of the $N_f = 3$ ChPT parameters, and will include a $\sim 26\%$ deviation from the 2-parameter fit with $F = 0.0531$ as a systematic error in the final results.

So far we have treated the strange quark mass fixed at $m_s = 0.080$ in the $N_f = 2 + 1$ studies. In fact, the combined fit of the degenerate $N_f = 3$ and $2 + 1$ results implies that Σ_{eff} in the chiral limit of m_{ud} changes by less than 1% when m_s varies between 0.060 and 0.100. We can, therefore, safely ignore the error due to a slight mismatch of the strange quark mass from its physical value. This weak sensitivity to m_s supports the assumption that the strange quark at the physical mass is almost decoupled from the low-energy theory and the use of the reduced $N_f = 2$ ChPT formula to fit the $N_f = 2 + 1$ lattice QCD data.
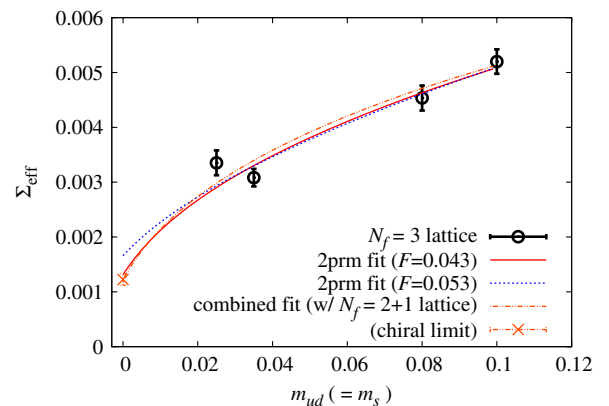

FIG. 11 (color online). Same as Fig. 9 but for the degenerate ($m_{ud} = m_s$) $N_f = 3$ QCD. Results of the 2-parameter fits and a combined $N_f = 3$ fit are plotted.

VII. SUMMARY AND CONCLUSION

Before quoting the final results, let us discuss the possible systematic errors.

Our simulation uses an exactly chiral-symmetric Dirac operator and has reached almost the chiral limit: $m_{ud} = 0.002$ for the $N_f = 2$ and $2 + 1$ runs, which corresponds to ~3 MeV in the physical unit. The NLO ChPT formula (5) is valid in both the ϵ and p regimes. As a result, the chiral extrapolation of Σ_{eff} in $N_f = 2$ and $2 + 1$ QCD is stable. As discussed in Sec. VI, by varying the fit range (and N_f in the ChPT formula for the $N_f = 2 + 1$ analysis), we estimate the systematic effects due to the chiral extrapolation as $(+3.7\%/-5.2\%)$ for Σ of $N_f = 2$ QCD and $(+6.5\%/-0.5\%)$ for Σ^{phys} of $N_f = 2 + 1$ QCD, respectively. The upper and lower limits come from the variation of Σ with the various fit schemes. We also found that the m_s dependence is negligible in the range $m_s = 0.060$–0.100, so that Σ^{phys} can be treated as the chiral condensate at the physical value of the strange quark mass.

On the other hand, for the degenerate $N_f = 3$ lattice data, our estimate for the systematic error in the chiral fit is larger because of the bad convergence of $N_f = 3$ ChPT and smaller number of data points. In fact, we observe that Σ moves as large as 26% depending on the fit schemes, from which we estimate the systematic error from this source to be $\pm 26\%$ for Σ in the $N_f = 3$ chiral limit.

The finite volume effects have also been discussed in the previous sections. For the $N_f = 2$ lattice results, we expect that a possible higher-order effect in the $1/L$ expansion beyond 1-loop ChPT is partly reflected in the difference among different topological sectors. We thus estimate the systematic error from this source to be $\pm 11\%$. For the $N_f = 2 + 1$ (and 3) case, we use more direct comparison with $L = 24$ lattice results and the systematic error is estimated as $(+0.9\%/-2.9\%)$. With a naive order counting, the leading finite volume effect is estimated as $1/(F^4 V)$, which is the 2-loop effect in the p expansion. With $F = 71$ MeV (see below), this gives a large value (~ 0.52) as the size of the 2-loop correction. In fact, including the numerical coefficient β_1 given in the Appendix the 1-loop correction is $\beta_1/(F^2 V^{1/2}) \sim -0.06$. If we assume that the numerical coefficient is

TABLE VII. Systematic errors for $[\Sigma^{\overline{\text{MS}}}(2 \text{ GeV})]^{1/3}$ and F. The total errors are obtained by adding each estimate by quadrature.

	$N_f = 2$ ChPT $[\Sigma]^{1/3}$	$N_f = 3$ ChPT $[\Sigma^{\text{phys}}]^{1/3}$	$[\Sigma]^{1/3}$	F
renormalization	$^{+1.4}_{-1.1}\%$	$^{+1.2}_{-1.1}\%$	$^{+1.2}_{-1.1}\%$	$\cdots$
chiral fit	$^{+1.2}_{-1.8}\%$	$^{+2.2}_{-0.2}\%$	$\pm 8.7\%$	$\pm 8.0\%$
finite volume	$\pm 3.7\%$	$^{+0.3}_{-1.0}\%$	$^{+0.3}_{-1.0}\%$	$\pm 3.0\%$
finite a	$\pm 7.0\%$	$\pm 7.0\%$	$\pm 7.0\%$	$\pm 7.0\%$
total	$^{+8.1}_{-8.2}\%$	$^{+7.4}_{-7.2}\%$	$\pm 11\%$	$\pm 11\%$

also small (~ 0.05) at the 2-loop order, this naive estimate gives a 3% effect, which is in the same ball park as the estimate given above. The small numerical coefficient at the 2-loop level is indeed obtained in a recent study [42].

Since our lattice studies are done at only 1 value of β, it is difficult to estimate the size of discretization effects. It should be partly reflected in the mismatch of the observables measured in different ways. For instance, the inverse lattice spacing determined from the ϕ-meson mass, $1/a = 1.774(17)$ GeV, is 1% larger than the determination from the Ω-baryon mass, $1/a = 1.759(10)$ GeV [35]. The latter corresponds to the Sommer scale $r_0 = 0.51$ fm, which is higher than the nominal value 0.49 fm or the recently favored value 0.46–0.47 fm by about 4–10%. On the other hand, a naive order counting $(a\Lambda_{\text{QCD}})^2$ with $\Lambda_{\text{QCD}} \sim 450$ MeV suggests a systematic effect of ~7%, which is consistent with the above mismatch. We therefore add this naive estimate, $\pm 7\%$, as the systematic error due to finite lattice spacing.

We convert the value of the condensate to the definition in the standard renormalization scheme, i.e., the $\overline{\text{MS}}$ scheme. By using the nonperturbative renormalization technique through the RI/MOM scheme we obtained the Z factor in our previous work [43] as $1/Z_S(2 \text{ GeV}) = 0.804(10)(^{+25}_{-33})$ for $N_f = 2$ and $0.792(10)(^{+24}_{-26})$ for $N_f = 2 + 1$ and 3, where the errors are statistical and systematic, respectively.[2]

Including all the systematic effects above, which are summarized in Table VII, we obtain the chiral condensate of up and down quarks in their massless limit as

$$\Sigma^{\overline{\text{MS}}}(2 \text{ GeV}) = \begin{cases} [242(05)(20) \text{ MeV}]^3 & \text{for } N_f = 2 \text{ QCD} \\ [234(04)(17) \text{ MeV}]^3 & \text{for } N_f = 2 + 1 \text{ QCD (at physical } m_s), \\ [214(06)(24) \text{ MeV}]^3 & \text{for } N_f = 3 \text{ QCD (at } m_s = 0) \end{cases} \tag{15}$$

where the errors are again statistical and systematic, respectively. Here, the total systematic errors are obtained by adding each estimate by quadrature. Note that the result for $N_f = 2 + 1$ is slightly changed from [18] because a different input for the scale determination is used. We find a nontrivial m_s dependence on the chiral condensate: as the

strange quark mass goes down from $m_s = \infty$ ($N_f = 2$ QCD) to the chiral limit $m_s = 0$, the value of Σ decreases.

---

[2]The value for $N_f = 2 + 1$ is slightly changed from [43] due to the different determination of the lattice scale, that affects the renormalization group running of the Z factor.

TABLE VIII.   Numerical results for β_n for $T/L = 1, 2,$ and 3.

T/L	β_1	β_2	β_3	β_4	β_5	β_6
1	0.1405	-2.030×10^{-2}	-4.820×10^{-4}	2.531×10^{-5}	-2.238×10^{-6}	2.672×10^{-7}
2	0.083 60	-1.295×10^{-2}	-1.778×10^{-3}	3.265×10^{-4}	-9.120×10^{-5}	3.250×10^{-5}
3	$-0.041\,94$	$0.012\,15$	-9.508×10^{-3}	3.622×10^{-3}	-1.898×10^{-3}	1.248×10^{-3}

The chiral condensate determined in this work (15) is consistent with those in our previous results obtained from the pseudoscalar meson mass [20,40] and from the topological susceptibility [44–46]. A similar work done using the $N_f = 2$ Wilson fermion and the p regime ChPT [36] quoted $\Sigma^{\overline{\text{MS}}}(2 \text{ GeV}) = 276(3)(4)(5) \text{ MeV}$, which is slightly higher than our result. A recent work [47] in a mixed action approach (overlap valence + Wilson sea) has also reported a larger value. More detailed study would be necessary to understand the source of the discrepancy, if it is significant.

From the NLO terms, we also obtain

$$F = 71(3)(8) \text{ MeV} \quad \text{for } N_f = 3 \text{ QCD}, \qquad (16)$$

(or $\sqrt{2}F = 100(4)(11) \text{ MeV}$) and

$$L_6^r(770 \text{ MeV}) = \begin{cases} -0.000\,09(13)(30) & \text{for } N_f = 2 \text{ QCD}, \\ 0.000\,03(07)(17) & \text{for } N_f = 3 \text{ QCD}, \end{cases}$$
$$(17)$$

where the systematic errors are estimated in a similar manner. For F, their estimates are listed in Table VII while for L_6^r, the systematic error is dominated by the one from chiral extrapolation, as seen in Table III and IV. Although the accuracy for these quantities is not as good as that of the chiral condensate, they provide important consistency checks.

In this study, we have investigated the eigenvalue spectrum of the QCD Dirac operator, which is free from ultraviolet power divergences. The lattice QCD results show a good agreement with the ChPT calculation at NLO in the region of λ less than $m_s^{\text{phys}}/2$. In particular, the effect of pion-loop, or the chiral logarithm, is clearly seen. The dependence on the volume V, the quark masses m_{ud} and m_s, and the topological charge Q is also well described by ChPT. Result for the chiral condensate extracted from this study is therefore robust, as the systematic errors are controlled except for that coming from the discretization effect.

Our work has also addressed a nontrivial flavor dependence of the chiral condensate. As the strange quark mass is reduced towards the chiral limit, its dynamical effect is seen as lowering the value of Σ.

ACKNOWLEDGMENTS

APPENDIX A: SHAPE COEFFICIENT β_n

In (10), we need to calculate the coefficients β_n [30], which depend only on the shape of the four-dimensional box. The definition of β_n is given by

$$\beta_n \equiv \left(\frac{-1}{4\pi}\right)^n \left(\alpha_n + \frac{2}{n(n-2)}\right) (n \neq 2),$$
$$\beta_2 \equiv \frac{\alpha_2 - \ln 4\pi + \gamma - 3/2}{16\pi^2}, \qquad (A1)$$

$$\alpha_n \equiv \int_0^1 dt \left\{ t^{n-3}\left(S\left(\frac{L^2}{V^{1/2}t}\right)^3 S\left(\frac{T^2}{V^{1/2}t}\right) - 1\right) \right.$$
$$\left. + t^{-n-1}\left(S\left(\frac{V^{1/2}}{L^2 t}\right)^3 S\left(\frac{V^{1/2}}{T^2 t}\right) - 1\right) \right\}, \qquad (A2)$$

$$S(x) \equiv \sum_{k=-\infty}^{\infty} \exp(-\pi k^2 x), \qquad (A3)$$

where $\gamma \sim 0.577\,215\,665 \cdots$ is the Euler's constant. Here the summation in $S(x)$ is well approximated by a truncation $|k| \leq 20$. For the case with $T/L = 1, 2,$ and 3, the numerical values of β_n are listed in Table VIII.

[1] S. Weinberg, Phys. Rev. **166**, 1568 (1968).

[2] J. Gasser and H. Leutwyler, Ann. Phys. (N.Y.) **158**, 142 (1984); Nucl. Phys. **B250**, 465 (1985).

[3] T. Banks and A. Casher, Nucl. Phys. **B169**, 103 (1980).

[4] P. H. Damgaard and H. Fukaya, J. High Energy Phys. 01 (2009) 052.

[5] P. H. Damgaard and S. M. Nishigaki, Nucl. Phys. **B518,** 495 (1998).

[6] T. Wilke, T. Guhr, and T. Wettig, Phys. Rev. D **57,** 6486 (1998).

[7] G. Akemann and P. H. Damgaard, Nucl. Phys. **B528,** 411 (1998).

[8] P. H. Damgaard and S. M. Nishigaki, Phys. Rev. D **63,** 045012 (2001).

[9] A. V. Smilga and J. Stern, Phys. Lett. B **318,** 531 (1993).

[10] J. C. Osborn, D. Toublan, and J. J. M. Verbaarschot, Nucl. Phys. **B540,** 317 (1999).

[11] H. Neuberger, Phys. Lett. B **417,** 141 (1998);

[12] H. Neuberger, Phys. Lett. B **427,** 353 (1998).

[13] P. H. Ginsparg and K. G. Wilson, Phys. Rev. D **25,** 2649 (1982).

[14] M. Luscher, Phys. Lett. B **428,** 342 (1998).

[15] H. Fukaya *et al.* (JLQCD and TWQCD Collaborations), Phys. Rev. Lett. **98,** 172001 (2007).

[16] H. Fukaya *et al.* (JLQCD and TWQCD Collaborations), Phys. Rev. D **76,** 054503 (2007).

[17] S. Aoki *et al.* (JLQCD Collaboration), Phys. Rev. D **78,** 014508 (2008).

[18] H. Fukaya, S. Aoki, S. Hashimoto, T. Kaneko, J. Noaki, T. Onogi, and N. Yamada (JLQCD collaboration), Phys. Rev. Lett. **104,** 122002 (2010); **105,** 159901(E) (2010).

[19] H. Fukaya (JLQCD and TWQCD Collaborations), Proc. Sci., LAT2009 (2009) 004 [arXiv:1001.1786].

[20] J. Noaki *et al.* (JLQCD and TWQCD Collaborations), Proc. Sci., LAT2009 (2009) 096 [arXiv:0910.5532].

[21] H. Fukaya *et al.* (JLQCD Collaboration), Phys. Rev. D **74,** 094505 (2006).

[22] T. DeGrand, Z. Liu, and S. Schaefer, Phys. Rev. D **74,** 094504 (2006); **74,** 099904(E) (2006).

[23] C. B. Lang, P. Majumdar, and W. Ortner, Phys. Lett. B **649,** 225 (2007).

[24] P. Hasenfratz, D. Hierl, V. Maillart, F. Niedermayer, A. Schafer, C. Weiermann, and M. Weingart, J. High Energy Phys. 11 (2009) 100.

[25] T. DeGrand and S. Schaefer, Phys. Rev. D **76,** 094509 (2007).

[26] O. Bar, S. Necco, and A. Shindler, J. High Energy Phys. 04 (2010) 053.

[27] K. Jansen and A. Shindler, Proc. Sci., LAT2009 (2009) 070 [arXiv:0911.1931].

[28] A. Hasenfratz, R. Hoffmann, and S. Schaefer, Phys. Rev. D **78,** 054511 (2008).

[29] C. Bernard (MILC Collaboration), Phys. Rev. D **65,** 054031 (2002).

[30] P. Hasenfratz and H. Leutwyler, Nucl. Phys. **B343,** 241 (1990).

[31] Y. Iwasaki, Nucl. Phys. **B258,** 141 (1985).

[32] T. Izubuchi and C. Dawson (RBC Collaboration), Nucl. Phys. B, Proc. Suppl. **106–107,** 748 (2002).

[33] P. M. Vranas, Phys. Rev. D **74,** 034512 (2006).

[34] P. Hasenfratz, V. Laliena, and F. Niedermayer, Phys. Lett. B **427,** 125 (1998).

[35] J. Noaki *et al.* (JLQCD and TWQCD collaborations) (unpublished).

[36] L. Giusti and M. Luscher, J. High Energy Phys. 03 (2009) 013.

[37] R. Brower, S. Chandrasekharan, J. W. Negele, and U. J. Wiese, Phys. Lett. B **560,** 64 (2003).

[38] S. Aoki, H. Fukaya, S. Hashimoto, and T. Onogi, Phys. Rev. D **76,** 054508 (2007).

[39] S. Aoki and H. Fukaya, Phys. Rev. D **81,** 034022 (2010).

[40] J. Noaki *et al.* (JLQCD and TWQCD Collaborations), Phys. Rev. Lett. **101,** 202004 (2008).

[41] H. Fukaya *et al.* (JLQCD Collaboration), Phys. Rev. D **77,** 074503 (2008).

[42] C. Lehner, S. Hashimoto, and T. Wettig, J. High Energy Phys. 06 (2010) 028.

[43] J. Noaki *et al.* (JLQCD and TWQCD Collaborations), Phys. Rev. D **81,** 034502 (2010).

[44] T. W. Chiu *et al.* (JLQCD and TWQCD Collaborations), Proc. Sci., LATTICE2008 (2008) 072 [arXiv:0810.0085].

[45] T. W. Chiu, T. H. Hsieh, and P. K. Tseng (TWQCD Collaboration), Phys. Lett. B **671,** 135 (2009).

[46] S. Aoki *et al.* (JLQCD and TWQCD Collaborations), Phys. Lett. B **665,** 294 (2008).

[47] F. Bernardoni, P. Hernandez, N. Garron, S. Necco, and C. Pena, arXiv:1008.1870.